Volume 1 | Number 1 | Jan 2013 | Pages 1–100

Journal of
Materials Chemistry A

Materials for energy and sustainability
www.rsc.org/materialsA

Li⁺

ROYAL SOCIETY
OF CHEMISTRY

ROYAL SOCIETY
OF CHEMISTRY

www.rsc.org/materialsA

Type 1 = 10.94% PCE   Type 2 = 6.39% PCE   Type 3 = 12.03% PCE

Journal of Material Chemistry A

Light Management: Porous 1-Dimensional Nanocolumnar Structures as effective Photonic Crystal for Perovskite Solar Cells

F. Javier Ramos,[a] Manuel Oliva-Ramírez,[b] Mohammad Khaja Nazeeruddin,[c] Michael Graetzel,[c] Agustín R. González-Elipe[b] and Shahzada Ahmad[a]

Hybrid organic-inorganic perovskite solar cells is a topic with an increasing interest, as in a short time span they are able to lead in the third generation photovoltaics. Organohalide perovskites posses exceptional optoelectronic and physical properties, thus making possible its implementation in many diverse configurations of photovoltaic devices. In this work, we present three different configurations of porous 1-dimensional photonic crystals (1-DPC) based on alternated nanocolumnar layers of oxides with different refractive indices (n) that were deposited by Physical Vapor Deposition at Oblique Angle (PVD-OAD). They are implemented as the photoanode of $CH_3NH_3PbI_3$ solar cells to improve the management of the light into the device. These configurations improved the performance of the photovoltaic system designing a light intereference structure capable of enhancing the absorption capability of the perovskite. Devices fabricated using these photonic crystal structures presented an efficiency >12% (J_{SC}=18.77mA cm^{-2}; V_{OC}=1026mV; FF=0.617), in contrast with only 9.56±0.37% for a reference device based on non-photonic crystal TiO_2 layers deposited in analogous conditions.

Introduction

Organoleadhalide perovskites are being employed as semiconducting absorbers for solar cell applications[1,2]. Its ability to harvest light with very high molar extinction coefficient compared to organic sensitizers[3], low exciton binding energy[4,5], low non-radiative recombination[6,7] and ambipolar nature of high electron and hole conduction[8,9] has revolutionized thin film based photovoltaics. This is being seen as a cost effective solution for sustainability of our planet[10,11]. Power conversion efficiencies (PCE) made a stunning progress in less than 5 years[12–16]. Devices with PCE in excess of 10% can be easily fabricated in diverse architectures and choice of materials[17–21]. However, most of the research efforts are centered on state of the art materials and its ability to further push the PCE.

On the other hand, photonic crystalsare known for their ability to selectively localize the light electrical field strength[22] Depending on the number of directions where the periodic alternation of the refractive index occurs, photonic crystals are classified in: 1-dimensional (1D), 2-dimensional (2D) and 3-dimensional (3D) ones[23]. The utilization of 1-dimensional

photonic crystal (1-DPC) structures where the periodic modulation of the refractive index arises in the same direction the light goes through, has been a concept successfully employed in order to tune the photocurrent in solar cells[24,25]. Consequently, photonic crystal have been used in several photovoltaic applications such as dye-sensitized solar cells (DSSCs)[26,27], solid-state-DSSCs (ss-DSSCs)[28] and, more recently, in perovskite solar cell [29,30] where their working principles have been reported[31]. Light dispersion effects based on light scattering have also been claimed as contributing to the performance of DSSCs[22,32,33]. IIn the recent past, the introduction of photonic crystal structures in perovskite solar cells has been exploited basically for tuning the color of the devices but at the expense of the photocurrent and consequently PCE values[29,30]. The researchers were able to show a wide color palette but the measured PCE was 8.8% for the champion cell[29] and 3.86% when an optical cavity behind the back electrode was introduced[30].

The implementation of nanostructured 1D architectures, such as nanoribbons, nanowires, nanorods and nanocolumns with high aspect ratio and high surface-to-volume relation to increase either collection or transport properties, have also been extensively explored in diverse electro-optical applications and in different types of solar cells[34–39]. In particular, metal oxide nanostructured 1D architectures have been reported for perovskite solar cells using a variety of techniques well known and established in literature such as ZnO by chemical bath deposition[40], ZnO by plasma-enhanced chemical vapour deposition (PE-CVD)[41], TiO_2 by chemical bath deposition (solvothermally grown)[42–44], TiO_2 by electrospinning[45], electrospun lead-doped TiO_2 nanofibers with in situ perovskite synthesis[46] and TiO_2 by physical vapour

a. Abengoa Research, Abengoa, C/Energía Solar no 1, Campus Palmas Altas, 41014, Sevilla, Spain. E-mail: shahzada.ahmad@abengoa.com
b. Instituto de Ciencia de Materiales de Sevilla, (CSIC-Universidad de Sevilla), C/Americo Vespucio 49, 41092 Sevilla, Spain
c. Laboratory of Photonics and Interfaces, Department of Chemistry and Chemical Engineering, École Polytechnique Fédérale de Lausanne, Station 6, CH-1015 Lausanne, Switzerland
† Footnotes relating to the title and/or authors should appear here.
Electronic Supplementary Information (ESI) available: [details of any supplementary information available should be included here]. See DOI: 10.1039/x0xx00000x

deposition at oblique angles (PVD-OAD)[47,48]. From these techniques, those where a solvent bath is not required, i.e. electrospinning, PE-CVD and PVD-OAD, are deemed industrially scalable processes in a facile manner due to their ability to uniformly coat large area surfaces.

Usually, in the field of photonic crystals, 1D nanostructures have been applied to fabricate 2-DPC, where the periodic modulation of the refraction index of the system is controlled by the distance between columns or rods[23]. Unlike this topography, planar 1-DPCs in the form of porous Bragg reflectors prepared by PVD-OAD are formed by the arrangement of 1D nano-structural units in the form of a film and consist of an alternating stack of nanocolumnar porous layers with different refractive indices. Recently, this type of architectures have been applied for optofluidic analysis[49] and to increase the efficiency of DSSCs[50,51]. However, to the best of our knowledge, 1-DPC made by alternating 1D porous nanostructured films prepared by PVD-OAD haven't been explored for perovskite solar cells applications.

Herein, as a proof of concept on the perovskite solar cell performance, we study the effect of using photoanodes consisting of alternate nanocolumnar layers of porous oxides to induce photonic crystal-like effects in the modulation of light[52]. To obtain a precise and homogeneous arrangement of the different nanocolumnar layers, the PVD-OAD technique was selected for their preparation.

Particularly, three different types of nanostructured 1-DPCs were fabricated and compared with similar structures where light confinements due to photonic crystal effects are not expected. Photonic Crystal type 1 (PC1) consists of 5 stacked porous layers of nanocolumnar TiO_2 with alternant refractive indices. The principle applied to systematically vary the refraction index of the same material from one layer to the next was to adjust the incident zenithal angle (α) of deposition. This parameter is known to induce a variation in the porosity of the films prepared by this method and, consequently, in the refractive index of the film. [50,51,53] According to the effective medium approximation theory[54], an increase in porosity leads to a decrease in refraction index (n). In PC1 the TiO_2 layers, deposited at $\alpha=60°$ and $\alpha=85°$, had a thickness of 75nm and approximate refraction indices of $n=1.80$ and $n=1.63$, respectively. The selection of a TiO_2 anode of approximately 5×75nm thickness was dictated by previous results[48] where a maximum efficiency of the perovskite solar cell was found for a similar thickness of a homogeneous TiO_2 anode prepared by PVD-OAD. For Photonic Crystal type 2 (PC2) and Photonic Crystal type 3 (PC3), the alternation in refractive index was not due to changes in the angle of deposition and therefore in the porosity of a single material, but to the alternation of two materials presenting different refraction indices. In PC2 and PC3 alternated porous TiO_2 and SiO_2 layers were employed to create a photonic crystal-like effect while keeping the tilting angle of the nanostructures and the film porosity constant from one layer to the next. More importantly it was found that the incorporation of a non-electron injecting photoanode material like SiO_2 did not affect significantly the cell performance, an effect that must be attributed to the high

diffusion length of excimers in perovskite materials. In any case, the control of the thickness of each individual layer, the number of layers, the variation in their refractive indices and the optical interference effects of these 1-DPC with the FTO substrates were designed to cover the absorption spectral region of the perovskite,. This effect should contribute to the total absorption of the film and to enhance the generated photocurrent. Unlike previous reports[29,30], herein we were not only able to fabricate different photoanodes based on the tailored designed photonic crystals, but also to improve the light harvesting capabilities and final performance of the fabricated perovskite solar cells. Photovoltaic behaviour (J_{SC} and PCE) of the solar cells prepared in the present work with PC1 (J_{SC}=19.29mA cm^{-2}; PCE=10.94%) and PC3 (J_{SC}=18.77mA cm^{-2}; PCE=12.03%) resulted much improved with respect to similar TiO_2 tilted nanocolumnar photoanodes deposited by PVD-OAD[48] (J_{SC}=18.25mA cm^{-2}; PCE=10.22%). It must be stressed that due to the rational design of the photonic crystal, the obtained photocurrents and efficiencies were higher than state of the art values of other perovskite solar cells containing photonic crystals[29]. In this regard, it is also worth noting the additional advantages of the PVD-OAD procedure for series fabrication due to its facile and easy scalability at industrial level.

Results and discussion

Morphology and optical characteristics of 1-DPCs

For a comprehensive visualization, Figures 1a-c present in the form of schemes the different architectures of the perovskite solar cells essayed in the present work that are characterized by different photonic crystal structures. For comparison purposes, the schematic configuration of the TiO_2 nanocolumnar photoanodes employed as reference are included in the supporting information (Figure S1). These schemes are complemented in Figures 1d-f by a detailed summary of key characteristics and properties of the prepared photonic crystal films, such as type of material and thickness, number of layers, glancing angle of deposition employed during PVD-OAD (α) and refractive index of each single layer (n). According to Figure 1a, PC1 consists of 5 nanocolumnar layers of TiO_2 prepared at two alternating deposition angles. This procedure is known to change the porosity of the individual layers and hence their refractive index[53]. For PC2 (Figure 1b) a compact layer of TiO_2 was first deposited to act as both buffer layer and first layer of the PC structure due to its high refractive index. Then, it followed a porous nanocolumnar SiO_2 (low n) layer and, on the top, another nanocolumnar TiO_2 layer deposited by keeping fix the deposition angle (α). Here, the different refraction indices of SiO_2 and TiO_2 induce an interference effect typical of 1-DPC. In a similar fashion, PC3 alternates nanocolumnar TiO_2 and SiO_2 layers prepared at the same deposition angle α and characterized by a similar porosity. In this case the bottom layer consisted of a nanocolumnar TiO_2 film prepared at oblique angle and an

additional very thin buffer under layer made by spray pyrolysis deposition (SPD) had to be incorporated. More details about porosity of each film can be found in the experimental section. Figures 1g-I illustrates the transmittance spectra of the
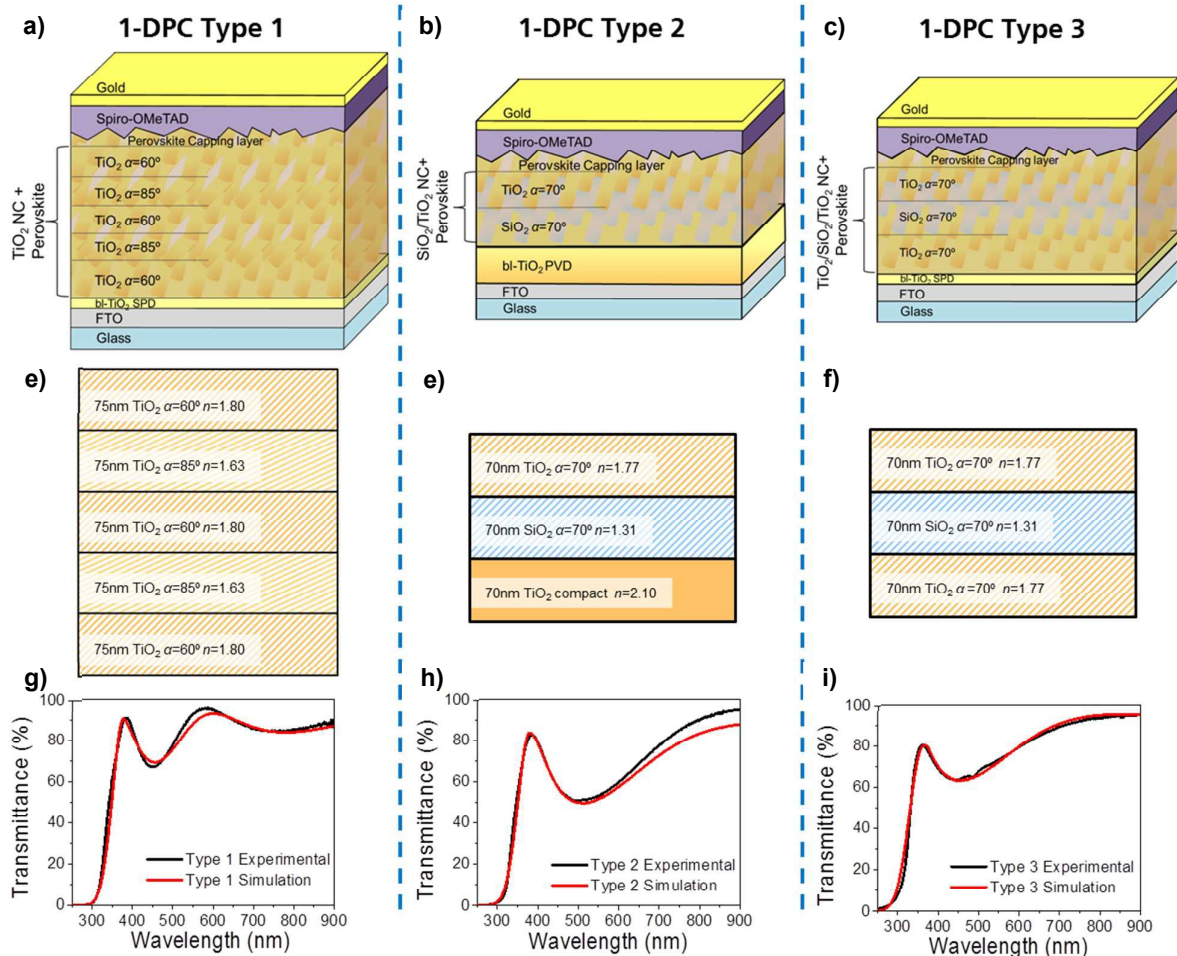

Figure 1. a-c) Architectures of the final devices containing 1-dimensional photonic crystal (1-DPC) Type 1, 2 and 3 respectively (not at scale). **d-f)** Schematic representation of the photonic crystals type 1, 2 and 3 respectively indicating composition of the film, thickness, deposition glancing angle (α) and refractive index of each monolayer. **g-i)** Experimental transmittance measurements (black lines) and simulations (red ones) for the different 1-DPC structures. Thickness dimensions are not at scale.

prepared photonic crystal films deposited onto quartz substrates. A well agreement was found between the experimental spectra and the simulated curves under the assumption of a constant value of the refraction index along the thickness of each single layer. The small discrepancies should be attributed to small deviations in porosity (and therefore refraction index) along each layer thickness, a variation that is common in PVD-OAD thin films. In the three spectra it is apparent a band in the 400-450nm region, coincident with the wavelengths where perovskite light harvesting is maximum. Although the purpose of the present work is not to carry out a precise description of the light confinement effects within the film structure, it is worth noting that the optical behaviour of the cell should also take into account the interference effects between the 1-DPC and the underlying FTO layer in the substrate. The resulting light interference and dispersion effects show that a decrease in

transmission occurs in a spectral region covering the whole visible range of the spectrum (experimental and simulated spectra are reported as supporting information S2a-c) encompassing the whole absorption band of the perovskite (supporting information S2d a comparison of the transmission spectra of the 1-DPC/FTO system before and after infiltration with the perovskite).

Pictures of the different types of studied photonic crystals deposited onto quartz are included in the supporting information (Figure S3), showing a certain coloration of these films. In summary, the final designs of the PCs was as follows: PC1 is ~375nm thick with alternating layers of TiO_2 with n=1.80 and n=1.63; PC2 is around 210nm, being composed of: a 70nm thick dense TiO_2 monolayer (n=2.10) and equivalent porous nanocolumnar SiO_2 (n=1.31) and TiO_2 (n=1.77) films with a total mesoporous thickness of 140 nm; PC3 is also about 210nm having three equivalent layers of alternated porous

nanocolumnar TiO$_2$ (n=1.77) and SiO$_2$ (n=1.31). Figure 2a represents a scheme of the geometrical arrangement used for the preparation of the different layers by PVD-OAD, where the evaporation angle is controlled by the position of the substrate regarding the evaporation source. PC1 was design as such to be relatively thicker (5 layers) than PC2 and PC3, as here the change in n was created by same materials just by changing the porosity and the variation in n was relatively lower than TiO$_2$/SiO$_2$ alternation. However the infiltration of perovskite was not found to be an issue for any of the configurations studied here as the total thickness in all the case remains <500nm.[48]

Scanning electron microscopy (SEM) was employed to confirm the porous and nanocolumnar microstructure of the different PCs. Figure 2b shows a cross section SEM micrograph taken with secondary electrons for a ca. 300nm thick TiO$_2$ tilted nanocolumnar film deposited on silicon. A similar film deposited on FTO has been employed here to fabricate a reference cell with no photonic crystal-like effect. Here an accurate control in the deposition angle of the nanocolumnar film is maintained along the layer.

Figures 2c and 2d correspond to a PC1 film deposited on silicon and reveal a clear distinction between the TiO$_2$ layers deposited at 60° and 85° and slightly different inclinations and widths when passing from one layer to the next. The high porosity evidenced by this micrograph clearly demonstrates that PC1 film could be used in a similar manner than the homogenous TiO$_2$ film for perovskite infiltration[48]. Figure 2e-2f shows the cross section of the PC2

secondary electrons for 300nm thick straight TiO$_2$ (α=70°) nanocolumns prepared onto Silicon wafer. **c-d)** Cross FE-SEM using back scattered electrons and secondary electrons respectively for Photonic Crystal type 1 over Si. **e-f)** Cross FE-SEM of back scattered electrons and secondary electrons respectively for PC2 onto Si. **g-h)** Cross FE-SEM by back scattered electrons and secondary electrons respectively for PC3 over Si.

film. In the backscattered SEM picture (Fig. 2e) the darker and lighter zones reveal the different material, SiO$_2$ and TiO$_2$ respectively, of each constituent layer (TiO$_2$ backscatters electrons more effectively than SiO$_2$ due to the higher atomic weight of Ti). The expected thickness of 210nm, with a highly porous layer of 140nm, due to both TiO$_2$ and SiO$_2$, can be clearly visualized in the images. Similarly, figures 2g-h clearly depicts the stack of different material layers employed for the fabrication of PC3. A general tendency that can be deduced from most of these images is that the nanocolumns progressively open and become wider when moving from the bottom to the top of the films. This is a common evolution in OAD films that is attributed to an increase in width of some nanocolumns at the expense of other that stop growing[55]. This tendency is in part responsible for the inaccuracies found between simulated and experimental transmission spectra of the different 1-DPC (Figure 1g-i).

Before finishing the solar cells fabrication, top view SEM images were taken before and after perovskite deposition. This comparative analysis of the capping layer morphology on top for the different photonic crystals showed no significant differences depending on photonic crystal photoanodes (supporting information, Figure S4). Additionally, cross-sectional SEM micrographs taken for the photoanodes after perovskite infiltration and for the final solar cells prepared with the three photonic crystals), confirmed that the underlying 1DPC photoanodes did not affect the morphology and crystal properties of the perovskite capping layer that, in all cases, was characterized by the same thickness and a similar size and cuboid shape of the perovskite crystals (supporting information Figure S5).

Perovskite solar cells using 1-DPCs as photanodes

The three types of photonic crystal films were used as host to distribute the perovskite absorber through their pore structure and atop it in the form of an homogeneous and pin-hole free capping layer (Figure S4 and S5 in the supporting information). The experimental strategy adopted was similar to that previously reported for us using single TiO$_2$ PVD-OAD films as anodes[48].

To assess their application in the photovoltaic devices, current-voltage characterization curves (*J-V*) and incident photon-to-current efficiency (*IPCE*) were recorded for the fabricated solar cells. In Table 1, results are summarized indicating average values and their
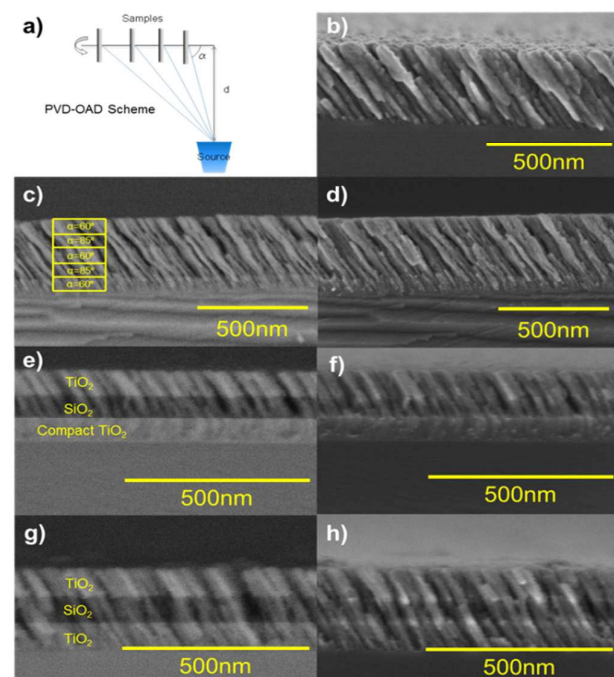

Figure 2. a) Schematic representation of the Physical Vapour Deposition at Oblique Angle (PVD-OAD) technique here employed to fabricate photonic crystal architectures. **b)** Cross sectional field effect scanning electron microscopy images (FE-SEM) using
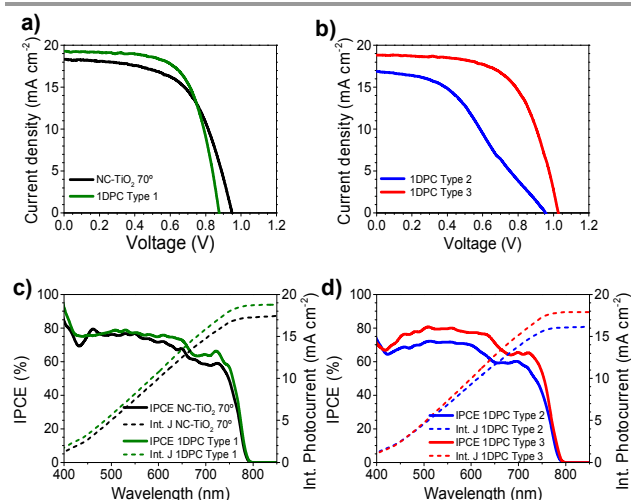
Figure 3. a) *J-V* characterization of the PSC containing TiO$_2$ tilted nanocolumns at α=70° (black) and PC1 (green). a) *J-V* characterization of the PSC containing PC2 (blue) and PC3 (red). c) *IPCE* spectra for the PSC with TiO$_2$ tilted nanocolumns at α=70° (black) and PC1 (green). d) IPCE spectra for the PSC with PC2 (blue) and PC3 (red).

standard deviations together with the best values attained (in brackets), for the following parameters: short-circuit current (J_{SC}), open-circuit voltage (V_{OC}), Fill factor (*FF*) and power conversion efficiency (*PCE*). For the best results achieved, the *J-V* curves and the *IPCE* spectra with the integrated photocurrent are reported in Figure 3. The increase in IPCE intensity in PC1 and, particularly, PC3 devices for practically the whole spectral region can be accounted for by light electrical field localization and dispersion effects occurring in the photonic crystal/FTO system[22,24,25,32,33]. The photonic behavior of the inorganic multilayer formed by the 1-DPC and the FTO is characterized by a lower transmission in a wide spectral zone (see supporting information S2) and supports that light interference and dispersion effects promoted by the photonic crystal / FTO ensemble can be the cause of the observed IPCE increases. Recent simulations of these light interference effects within the multilayer structure of 1-DPCs show a preferential localization of the light electrical field at given spatial depths and wavelengths[22] and may occur both

inside and just outside the Bragg reflector. They have been claimed as responsible for the increase in the photonic yield of DSSCs[24]. Hence, a similar effect is expected here, with the difference that in the studied in the perovskite based solar cells, the active absorbing phase distributes both within the photonic crystal and outside it and both regions can thus experience the effect of a preferential localization of light electrical field (see scheme in supporting information S6).

In the form of box-whisker plots, Figure 4 gathers the information for all studied devices. According to this figure, PC1 solar cells presented an enhanced absorption as compared to the reference TiO$_2$ nanocolumnar photoanode. Not only J_{sc} and IPCE of the champion PC1 (J_{SC} =19.29mA cm^{-2}) based solar cells is higher than the reference NC-TiO$_2$ based one (J_{SC} =18.25mA cm^{-2}), but also all of the samples prepared with PC1 (J_{SC} =18.56±0.55mA cm^{-2}) presented a higher J_{sc} than the average for the referenceTiO$_2$ anode (J_{SC} =17.87±0.53mA cm^{-2}). This better performance supports the idea that PC light management effects are the main factor contributing to the increase in IPCE. On the other hand, PC1 solar cells showed a slightly lower open circuit voltage (V_{OC}=867.7±11.92mV vs V_{OC}=934.4±10.71mV), possibly due to the more irregular interlayer shape which would create more trap sites and an intermittent contact between perovskite and TiO$_2$, contributing to increase the recombination processes in this case. This idea is supported by the comparison with the other photonic crystals structures, since PC1 showed the relative lowest voltage among all of them. Nevertheless, due to its higher IPCE, PC1 solar cells were more efficient (*PCE*=10.05±0.69%) than their analogous reference devices without PC effect (*PCE*=9.56±0.37%). For these series of magnitudes, it must be stressed the high reproducibility of the experiments for the twelve tested devices.

Table 1. Summary of the photovoltaic parameters (J_{SC}, V_{OC}, FF and PCE) obtained for the different perovskite solar cells here studied including 1D photonic crystal transparent anodes and its comparison with similar structures where photonic crystal effect is not expected. Maximum PCE values are in parenthesis.

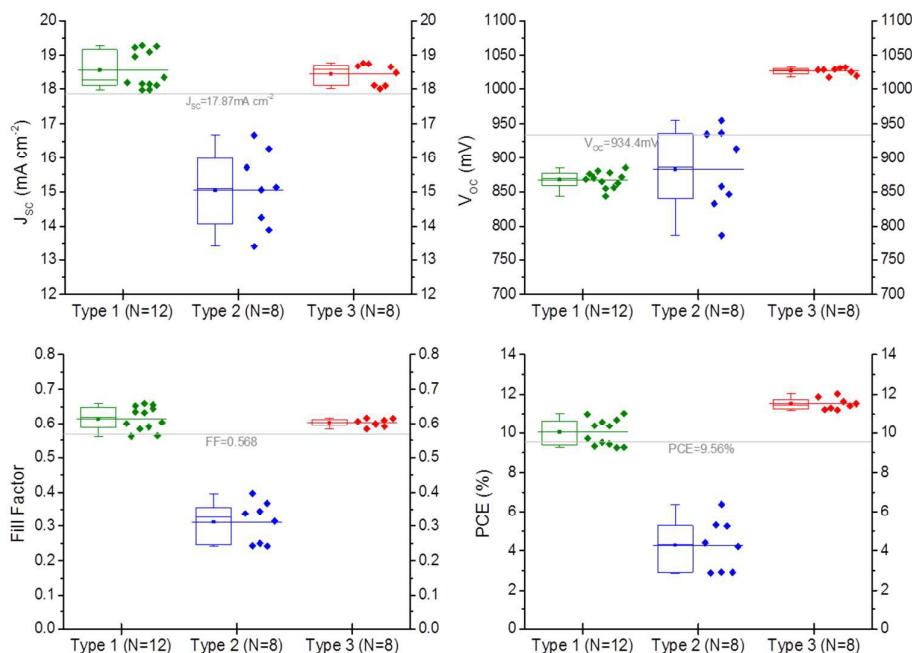|	J_{SC} (mA cm^{-2})	V_{OC} (mV)	Fill Factor	*PCE* (%)
NC-TiO$_2$[48]	17.87±0.532 (18.25)	934.4±10.71 (949.0)	0.568±0.02 (0.588)	9.56±0.37 (10.22)
PC1	18.56±0.554 (19.29)	867.7±11.92 (928.9)	0.615±0.03 (0.659)	10.05±0.7 (10.94)
PC2	15.05±1.152 (16.68)	883.1±60.28 (954.9)	0.312±0.06 (0.396)	4.28±1.32 (6.39)
PC3	18.44±0.322 (18.77)	1026.1±5.46 (1032)	0.603±0.02 (0.617)	11.52±0.30 (12.03)

Journal of Material Chemistry A

Figure 4. Box-whiskers plot which shows all the photovoltaic magnitudes for the different devices containing 1-DPC porous structures: PC1 (green), PC2 (blue) and PC3 (red). Grey lines represent the average values for each magnitude in the case of a reference TiO_2 nanocolumnar photoanode. Dots at the right of the box mean the exact value of each sample.

. In order to make the variation in the refractive index (n) more pronounced, photonic crystals structures PC2 and PC3 were fabricated with the introduction of nanocolumnar layers of SiO_2. For the PC2 devices, although the variation in "n" is quite high, the fabricated solar cells performed modestly with a PCE (J_{SC} =15.05±1.15mA cm^{-2}; V_{OC}=883.1±60.28mV; FF=0.312±0.06 and PCE=4.28±1.32%) lower than that of cells prepared on the PVD-OAD anodes. We relate this behavior with electronic factors, so that the incorporation of a non-electron injecting oxide (first layer of nanocolumnar porous SiO_2) just above the thick buffer layer of TiO_2 produces a distorted planar junction with extra series resistance and lower charge collection since carriers are transported slower by bulk perovskite (when non-injecting SiO_2 was employed directly onto buffer layer), than through semiconducting porous TiO_2 film (if injecting porous TiO_2 was the first monolayer onto buffer layer), resulting in a poor fill factor. To avoid this effect, in PC3, the first compact TiO_2 layer was replaced by a porous nanocolumnar film grown on a thin compact layer of this material deposited by spray pyrolysis. PC3 based devices shows the best PV properties in this work: J_{SC} = 18.44±0.32mAcm^{-2}; V_{OC}= 1026.1±5.46mV; FF=0.603±0.012 and PCE=11.52±0.3%. Photocurrent collection was clearly improved in comparison with the reference anode, although it was slightly lower than that found for PC1. The

substantial improvement in terms of voltage regarding reference and PC1 cells is explained by the reduction of the total thickness where perovskite absorber is infiltrated a feature that, limiting the recombination, allows achieving a better fill factor. Moreover, according to Figure 4, this structure has earned both a lower dispersion and a better performance, resulting in a competitive power conversion efficiency over 12% (J_{SC} =18.77mA cm^{-2}; V_{OC}=1032mV; FF=0.617 and PCE=12.03%).

Experimental section

Materials. Chemicals and solvents were purchased either from Sigma Aldrich or Agros and were used without any further treatment. Spiro-OMeTAD represented as 2,2',7,7'-tetrakis(N,N-di-p-methoxyphenyamine)-9,9-spirobifluorene (Spiro-MeOTAD) was purchased from Merck KGaA, while methylamine iodide, CH_3NH_3I (MAI), was synthetized according to the known literature.

Preparation of 1-DPC: In the case of alternate porous nanocolumnar layers of TiO_2 with different tilting angles (PC1), five layers around 75 nm thick (i.e total thickness of the film in the order of 375 nm) were prepared by PVD using an electron beam evaporator in an oblique angle deposition (PVD-OAD)

geometry. Details about this method of evaporation for TiO_2 materials can be found in previous publications[50,53,55]. Herein, to get stacked layers of different porosity and therefore refraction index, we have changed the zenithal angle of deposition (α) from 60° to 85° from one layer to the next.

The photonic crystals structures made of alternated nanocolumnar layers of SiO_2 and TiO_2, (PC2 and PC3) were also fabricated by means of the PVD-OAD technique. More detailed information about the use of this procedure to prepare this type of photonic structures can be found in previous works[49,52]. PC2 consists of a dense 70 nm thick TiO_2 layer prepared by PVD in a normal configuration ($\alpha=0^o$), followed by 70 nm thick SiO_2 and TiO_2 layers both prepared by PVD-OAD ($\alpha=70^o$) under similar deposition conditions. These two latter layers are porous and present a tilted nanocolumnar microstructure. For PC3 70nm thick alternating $TiO_2/SiO_2/TiO_2$ layers were deposited by PVD-OAD ($\alpha=70^o$) to create a PC-like structure formed by tilted nanocolumns. The determination of the refractive indices for the different architectures was carried out by UV-Vis absorption spectroscopy analysis of single layers of these materials directly prepared on quartz under equivalent geometrical configurations. UV-Visible spectra were recorded in transmission mode in a Cary 100 spectrometer. In the case of PC1, refractive indices of n=1.80 (porosity=45%) and n=1.63 (porosity=60%) were obtained for the TiO_2 nanocolumnar films prepared at $\alpha=60^o$ and $\alpha=85^o$, respectively. For PC2 the refractive indices obtained were n=2.1 for the first TiO_2 compact layer, n=1.31 (porosity=49%) for the SiO_2 nanocolumnar layer at $\alpha=70^o$, and n=1.77 (porosity=49%) for the TiO_2 nanocolumnar film at $\alpha=70^o$. Finally, for PC3 the refraction indices obtained were n=1.31 for the SiO_2 and n=1.77 for the TiO_2 nanocolumnar films both prepared at $\alpha=70^o$ and an approximate porosity of 49%. These porosity values were an approximation determined by means of an effective medium approximation considering that pores in the films were filled with air.

Films and photonic crystal structures were prepared on quartz substrates for UV-Vis absorption analysis, on silicon wafers for Scanning electron microscopy (SEM) observation and, onto FTO covered with a thin layer of compact TiO_2 prepared by spray pyrolysis for device fabrication (except in PC2 were the dense TiO_2 layer made by PVD also works as buffer layer). To induce the crystallization into the anatase phase of the TiO_2 films, a sequential annealing step (see device fabrication section) was applied to all architectures.

Simulation of the transmission spectra of the photonic crystal arrangement deposited on quartz or on the FTO substrate was carried out using a homemade code based on the transfer-matrix approach[56]. The code considered the typical Cauchy variation for the wavelength dependence of the refractive index of the films in the photonic crystal. The reported refractive indices and thicknesses of the porous layers obtained as an output of the fitting procedure agreed well with the values determined experimentally by the analysis of the single layers. Properly describing the optical gap of the system was the main criteria used for fitting. The same fitting parameters were used to simulate the transmission spectra of

the 1-DPC/FTO system, including in this case the thickness and refraction index of the FTO and some light dispersion effects described by Rayleigh dependence.

Device fabrication. FTO-coated glass was patterned by laser etching, followed by cleaning using Hellmanex solution and rinsed with deionized water and ethanol. Subsequently these substrates were ultrasonicated in 2-propanol and dried with compressed air. Prior the compact layer deposition, the substrates were treated with ultraviolet/O_3 for 30 minutes. When a thin compact TiO_2 layer was required (for PC1 and PC3 but not for PC2 because the bottom 70nm TiO_2 dense layer acts as buffer layer as well), a thin layer made of dense TiO_2 was deposited by spray pyrolysis at 450^oC using 1mL of titanium diisopropoxide bis(acetyl acetonate) precursor solution (75% in 2-propanol, Sigma Aldrich) in 19mL of pure ethanol using O_2 as carrier gas and, subsequently, samples were kept for further 30 minutes at 450^oC for the anatase formation. They were then allowed to attain room temperature and were subjected to a $TiCl_4$ treatment (dipping in a 0.02M $TiCl_4$ solution in deionized water at 70^oC for 30 minutes). The substrates were then washed with deionized water, fired at 500^oC for 15 minutes and cool down slowly. At that point, 1-DPCs were deposited using the previously described method. Before the perovskite deposition or before further characterization, 1-DPC electrodes were subjected to a sequential sintering step (5min at 125^oC, 5min at 325^oC, 5min at 375^oC, 15min at 450^oC and finally 30min at 500^oC) to form the anatase phase. Then, $CH_3NH_3PbI_3$ perovskite was sequentially deposited[14]. In this case, 1.25M lead iodide (PbI_2) was spun coated (6500rpm for 30s with 5500rpm s^{-1} as acceleration) using 50µL per cell of PbI_2 solution in N,N-dimethylformamide (DMF). To circumvent insolubility of PbI_2, the solution was previously dissolved in DMF at 115^oC and allowed to cool down to reach 70^oC temperature that was kept during the whole lead iodide deposition. After the PbI_2 deposition, the electrodes were heated at 70^oC for 15 minutes and cooled down to room temperature. The photoanodes containing PbI_2 were then dipped in MAI solution in 2-propanol (8mg mL^{-1}) for 20-25s, to allow the conversion in perovskite structure and the colour change from yellow to dark brown-black was observed. Afterwards they were rinsed in 2-propanol and dried using spin coater; finally they were annealed at 100^oC during 15 minutes. The selected hole transporting material (HTM), was Spiro-OMeTAD and it was spun coated at 4000rpm for 30s (acceleration 1650rpm s^{-1}). For this, 35µL of solution were dropped from a stock solution which was made by dissolving 72.3mg of Spiro-OMeTAD in 1mL of chlorobenzene; 21.9µL of tris(2-(1H-pyrazol-1-yl)-4-tert-butylpyrydine)cobalt(III)

bis(trifluoromethylsulphonyl)imide (FK209) stock solution (400mg of FK209 in 1mL of acetonitrile), 17.5µL of lithium bis(trifluoromethylsulphonyl)imide (LiTFSI) stock solution (520mg of LiTFSI in 1mL of acetonitrile) and 28.8µL of 4-tert-butylpyridine (tBP) were also added to the solution as additives. For the cathode, 80nm of gold were thermally evaporated atop of HTM under a vacuum level between 10^{-6} and 10^{-5}torr. PbI_2, MAI Spiro-OMeTAD solutions were prepared

inside an argon atmosphere (H_2O level :<1ppm and O_2 level: <10ppm). PbI_2 spin coating, glove box with moisture and oxygen controlled MAI dipping and HTM spin coating depositions were developed inside a dry box.

Characterization. For photovoltaic measurements 450W Xe lamp (Oriel) having a Schott K113 Tempax sunlight filter (Praezisions Glas & Optik GmbH) was the light source (around 100mW cm-2). For *J-V* measurements, digital source meter (Keithly Model 2400) was used to apply the voltage to the devices while current was recorded. For IPCE measurements, a 300W Xe lamp (ILC Technology) was coupled to a Gemini-180 double monochromator (Jobin Yvon Ltd.) to provide the desired light beam. A constant white light bias of 5% was applied to measure perovskite cells, using an array of white LEDS. SR830 model DSP lock-in amplifier (Standford Research Systems) was utilized to record the performance. Both for J-V and IPCE measurements the active area was fixed to 0.16cm^2 using a black mask. The surface and in-depth microstructure of the 1-DPC were observed by top-view and cross-sectional Field-emission SEM, respectively, using a Hitachi S5200 field-emission microscope operated at 5.0 keV. The transmittance spectra of the 1DPC were measured using the Cary 100 spectrometer.

Conclusions

Using oblique angle physical vapour deposition (PVD-OAD), three different types of 1-DPCs were deposited at low temperature. 1-DPC type 1 consists of 5 alternated layers of TiO_2 deposited at different incident angles to induce distinct porosities and refractive indices (*n*=1.80 & *n*=1.63), while for type 2 one dense layer of TiO_2 (*n*=2.10) followed by SiO_2 (*n*=1.31) and then nanocolumnar TiO_2 layer at α=70° (*n*=1.77). Type 3 photonic crystal was fabricated using $TiO_2/SiO_2/TiO_2$ with alternating refractive indices *n*=1.77/*n*=1.31/*n*=1.77, and gave the most efficient result studied here. We demonstrated the precise control growth of nanocolumnar photonic crystal thin films with a preferential orientation and a low concentration of defects. $CH_3NH_3PbI_3$ based semiconducting absorber was then infiltrated in these structures and solar cells were fabricated. PC1 solar cells showed performance of 10.94% PCE, while PC2 cells exhibited relatively low PCE up to 6.39%, which was even lower compare to a reference cell without photonic crystal effects. PC3 type cells showed the best performance here, and PCE in excess of 12% was measured.

In conclusion, we were able to fabricate perovskite solar cells with several photonic crystal structures more efficient than the state of the art cell. This improved behaviour has been attributed to the rational control of the photonic crystal/FTO system being tuned certain characteristics such as material selection, thickness of each individual layer, total number of layers and the variation in the refractive indices of each film. It is believed that these photonic effects maximize the light absorption of $CH_3NH_3PbI_3$ and lead to an enhancement in the J_{SC}. While *FF* was kept within reasonable values in these cell structures, the V_{OC} increased, leading to higher PCEs than in

reference cells with nanocolumnar films but without photonic crystal effects. We believe that the presented concept can be well utilized in the mixed perovskites structure to fabricate high performance solar cells, to and the approach will pave way to optimize the light management in perovskite solar cells.

References

1   S. Kazim, M. K. Nazeeruddin, M. Grätzel, and S. Ahmad, *Angew. Chem. Int. Ed.*, 2014, **53**, 2812–2824; *Angew. Chem., 2014,* **126***,* 2854-2867.
2   M. A. Green, A. Ho-Baillie, and H. J. Snaith, *Nature Photon.*, 2014, **8**, 506–514.
3   J. M. Frost, K. T. Butler, F. Brivio, C. H. Hendon, M. van Schilfgaarde, and A. Walsh, *Nano Lett.*, 2014, **14**, 2584–2590.
4   K. Tanaka, T. Takahashi, T. Ban, T. Kondo, K. Uchida, and N. Miura, *Solid State Commun.*, 2003, **127**, 619–623.
5   K. Tanaka, T. Takahashi, T. Kondo, K. Umeda, K. Ema, T. Umebayashi, K. Asai, K. Uchida, and N. Miura, *Jpn. J. Appl. Phys.*, 2005, **44**, 5923–5932.
6   E. Guillén, F. J. Ramos, J. A. Anta, and S. Ahmad, *J. Phys. Chem. C*, 2014, **118**, 22913–22922.
7   V. W. Bergmann, S. A. L. Weber, F. J. Ramos, M. K. Nazeeruddin, M. Grätzel, D. Li, A. L. Domanski, I. Lieberwirth, S. Ahmad, and R. Berger, *Nat. Commun.*, 2014, **5:5001**, 1–9.
8   G. Xing, N. Mathews, S. Sun, S. S. Lim, Y. M. Lam, M. Grätzel, S. Mhaisalkar, and T. C. Sum, *Science*, 2013, **342**, 344–7.
9   S. D. Stranks, G. E. Eperon, G. Grancini, C. Menelaou, M. J. P. Alcocer, T. Leijtens, L. M. Herz, A. Petrozza, and H. J. Snaith, *Science*, 2013, **342**, 341–4.
10 H. J. Snaith, *J. Phys. Chem. Lett.*, 2013, **4**, 3623–3630.
11 P. P. Boix, K. Nonomura, N. Mathews, and S. G. Mhaisalkar, *Mater. Today*, 2014, **17**, 16–23.
12 A. Kojima, K. Teshima, Y. Shirai, and T. Miyasaka, *J. Am. Chem. Soc.*, 2009, **131**, 6050–6051.
13 H.-S. Kim, C.-R. Lee, J.-H. Im, K.-B. Lee, T. Moehl, A. Marchioro, S.-J. Moon, R. Humphry-Baker, J.-H. Yum, J. E. Moser, M. Grätzel, and N.-G. Park, *Sci. Rep.*, 2012, **2:591**, 1–7.
14 J. Burschka, N. Pellet, S.-J. Moon, R. Humphry-Baker, P. Gao, M. K. Nazeeruddin, and M. Grätzel, *Nature*, 2013, **499**, 316–319.
15 N. J. Jeon, J. H. Noh, Y. C. Kim, W. S. Yang, S. Ryu, and S. Il Seok, *Nat. Mater.*, 2014, **13**, 897–903.
16 N. J. Jeon, J. H. Noh, W. S. Yang, Y. C. Kim, S. Ryu, J. Seo, and S. Il Seok, *Nature*, 2015, **517**, 476–480.
17 M. I. Dar, F. J. Ramos, Z. Xue, B. Liu, S. Ahmad, S. A. Shivashankar, M. K. Nazeeruddin, and M. Grätzel, *Chem. Mater.*, 2014, **26**, 4675–4678.
18 J. H. Noh, S. H. Im, J. H. Heo, T. N. Mandal, and S. Il Seok, *Nano Lett.*, 2013, **13**, 1764–1769.
19 A. Mei, X. Li, L. Liu, Z. Ku, T. Liu, Y. Rong, M. Xu, M. Hu, J. Chen, Y. Yang, M. Gratzel, and H. Han, *Science*, 2014, **345**, 295–298.
20 O. Malinkiewicz, A. Yella, Y. H. Lee, G. M. Espallargas, M. Graetzel, M. K. Nazeeruddin, and H. J. Bolink, *Nature Photon.*, 2013, **8**, 128–132.
21 D. Liu and T. L. Kelly, *Nature Photon.*, 2013, **8**, 133–138.

22 S. Nishimura, N. Abrams, B. a Lewis, L. I. Halaoui, T. E. Mallouk, K. D. Benkstein, J. Van De Lagemaat, and A. J. Frank, *J. Am. Chem. Soc.*, 2003, **125**, 6306–6310.

23 S. Robinson and R. Nakkeeran, in *Advances in Photonic Crystals*, ed. V. M. N. Passaro, InTech, 2013, pp. 3–26.

24 S. Colodrero, A. Mihi, J. a. Anta, M. Ocan, and H. Míguez, *J. P.hys. Chem. C*, 2009, **113**, 1150–1154.

25 L. González-García, S. Colodrero, H. Míguez, and A. R. González-Elipe, *Opt. Express*, 2015, **23**, 1642–1650.

26 D. Colonna, S. Colodrero, H. Lindström, A. Di Carlo, and H. Míguez, *Energy Environ. Sci.*, 2012, **5**, 8238.

27 C. López-López, S. Colodrero, M. E. Calvo, and H. Míguez, *Energy Environ. Sci.*, 2013, **6**, 1260.

28 J. T. Park, J. H. Prosser, D. J. Kim, J. H. Kim, and D. Lee, *ChemSusChem*, 2013, **6**, 856–64.

29 W. Zhang, M. Anaya, G. Lozano, M. E. Calvo, M. B. Johnston, H. Míguez, and H. J. Snaith, *Nano Lett.*, 2015, **15**, 1698–1702.

30 K.-T. Lee, M. Fukuda, S. Joglekara, and L. J. Guo, *J. Mater. Chem. C*, 2015, **3**, 5377–5382.

31 M. Anaya, G. Lozano, M. E. Calvo, W. Zhang, M. B. Johnston, H. J. Snaith, and H. Miguez, *J. Phys. Chem. Lett.*, 2015, **6**, 48–53.

32 B. P. G. O'Brien, N. P. Kherani, S. Zukotynski, G. A. Ozin, E. Vekris, N. Tetreault, A. Chutinan, S. John, A. Mihi, and H. Míguez, *Adv. Mater.*, 2007, **19**, 4177–4182.

33 I. Rodriguez, P. Atienzar, F. Ramiro-Manzano, F. Meseguer, A. Corma, and H. Garcia, *Phot. Nano. Fund. Appl.*, 2005, **3**, 148–154.

34 B. Tian, X. Zheng, T. J. Kempa, Y. Fang, N. Yu, G. Yu, J. Huang, and C. M. Lieber, *Nature*, 2007, **449**, 885–889.

35 P. Krogstrup, H. I. Jørgensen, M. Heiss, O. Demichel, J. V. Holm, M. Aagesen, J. Nygard, and A. Fontcuberta i Morral, *Nature Photon.*, 2013, **7**, 306–310.

36 Y. Liu, F. Zhang, and J. Wang, *Int. J. Photoenergy*, 2013, **Art. ID 34**, 1–6.

37 X. Feng, K. Shankar, O. K. Varghese, M. Paulose, T. J. Latempa, and C. A. Grimes, *Nano letters*, 2008, **8**, 3781–3786.

38 W.-Q. Wu, B.-X. Lei, H.-S. Rao, Y.-F. Xu, Y.-F. Wang, C.-Y. Su, and D.-B. Kuang, *Sci. Rep.*, 2013, **3:1352**, 1–7.

39 G. S. Han, S. Lee, J. H. Noh, H. S. Chung, J. H. Park, B. S. Swain, J.-H. Im, N.-G. Park, and H. S. Jung, *Nanoscale*, 2014, **6**, 6127–6132.

40 M. H. Kumar, N. Yantara, S. Dharani, M. Graetzel, S. Mhaisalkar, P. P. Boix, and N. Mathews, *Chem. Commun.*, 2013, **49**, 11089–91.

41 F. J. Ramos, M. C. López-Santos, E. Guillén, M. K. Nazeeruddin, M. Grätzel, A. R. González-Elipe, and S. Ahmad, *ChemPhysChem*, 2014, **15**, 1148–1153.

42 Q. Jiang, X. Sheng, Y. Li, X. Feng, and T. Xu, *Chem. Commun.*, 2014, **50**, 14720–14723.

43 H.-S. Kim, J.-W. Lee, N. Yantara, P. P. Boix, S. A. Kulkarni, S. Mhaisalkar, M. Grätzel, and N.-G. Park, *Nano Lett.*, 2013, **13**, 2412–2417.

44 J. Zhang and T. Pauporté, *ChemPhysChem*, 2015, **16**, 2836–2841.

45 S. Dharani, H. K. Mulmudi, N. Yantara, P. T. Thu Trang, N.-G. Park, M. Graetzel, S. Mhaisalkar, N. Mathews, and P. P. Boix, *Nanoscale*, 2014, **6**, 1675–1679.

46 Y. Xiao, G. Han, Y. Li, M. Li, and Y. Chang, *J. Mater. Chem. A*, 2014, **2**, 16856–16862.

47 J.-W. Lee, S. H. Lee, H.-S. Ko, J. Kwon, J. H. Park, S. M. Kang, N. Ahn, M. Choi, J. K. Kim, and N.-G. Park, *J. Mater. Chem. A*, 2014, DOI: 10.1039/C4TA04988H.

48 F. J. Ramos, M. Oliva-Ramirez, M. K. Nazeeruddin, M. Grätzel, A. R. Gonzalez-Elipe, and S. Ahmad, *J. Mater. Chem. A*, 2015, **3**, 13291–13298.

49 M. Oliva-Ramirez, L. Gonzalez-García, J. Parra-Barranco, F. Yubero, A. Barranco, and A. R. Gonzalez-Elipe, *ACS Appl. Mater. Interfaces*, 2013, **5**, 6743–6750.

50 L. González-García, I. González-Valls, M. Lira-Cantu, A. Barranco, and A. R. González-Elipe, *Energy Environ. Sci.*, 2011, **4**, 3426–3435.

51 L. González-García, J. Idígoras, A. R. González-Elipe, A. Barranco, and J. A. Anta, *J. Photochem. Photobiol. A*, 2012, **241**, 58–66.

52 L. González-García, G. Lozano, A. Barranco, H. Míguez, and A. R. González-Elipe, *J. Mater. Chem.*, 2010, **20**, 6408.

53 L. González-García, J. Parra-Barranco, J. R. Sánchez-Valencia, A. Barranco, A. Borrás, A. R. González-Elipe, M.-C. García-Gutiérrez, J. J. Hernández, D. R. Rueda, and T. a Ezquerra, *Nanotechnology*, 2012, **23**, 205701.

54 D. E. Aspnes, *Thin Solid Films*, 1982, **89**, 249–262.

55 A. Barranco, A. Borras, A. R. Gonzalez-Elipe, and A. Palmero, *Prog. Mater. Sci.*, 2016, **76**, 59–153.

56 M. Bass, in *Handbook of Optics, Fundamentals, Techniques and Design*, Mc Graw-Hill Inc., New York, 1995, p. Vol. 1 p.34.

Journal of Materials Chemistry A Accepted Manuscript